J. Am. Soc. Mass Spectrom. (2018) 29:1284–1294
DOI: 10.1007/s13361-018-1925-y

FOCUS: MASS SPECTROMETRY IN GLYCOBIOLOGY AND RELATED FIELDS: RESEARCH ARTICLE

Comprehensive Characterization of Swine Cardiac Troponin T Proteoforms by Top-Down Mass Spectrometry

Ziqing Lin,[1,2] Fang Guo,[1,3] Zachery R. Gregorich,[1] Ruixiang Sun,[1,4] Han Zhang,[5] Yang Hu,[1] Dhanansayan Shanmuganayagam,[6] Ying Ge[1,2,5]

[1]Department of Cell and Regenerative Biology, University of Wisconsin-Madison, Madison, WI 53705, USA
[2]Human Proteomics Program, University of Wisconsin-Madison, Madison, WI 53705, USA
[3]Department of Cardiology, Shandong Provincial Hospital, Jinan, 250021, Shandong, People's Republic of China
[4]Institute of Computing Technology, Chinese Academy of Sciences, Beijing, 100190, People's Republic of China
[5]Department of Chemistry, University of Wisconsin-Madison, Madison, WI 53706, USA
[6]Department of Animal Science, University of Wisconsin-Madison, Madison, WI 53706, USA

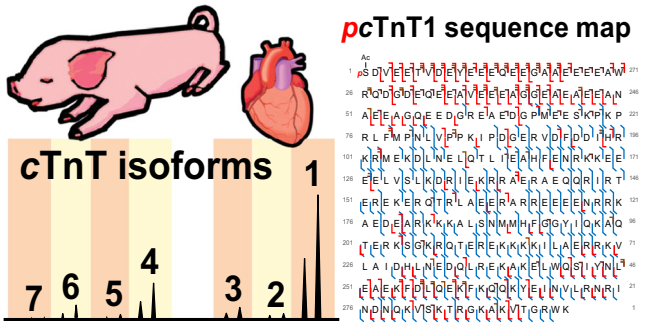

Abstract. Cardiac troponin T (*c*TnT) regulates the Ca^{2+}-mediated interaction between myosin thick filaments and actin thin filaments during cardiac contraction and relaxation. *c*TnT is released into the blood following injury, and increased serum levels of the protein are used clinically as a biomarker for myocardial infarction. Moreover, mutations in *c*TnT are causative in a number of familial cardiomyopathies. With the increasing use of large animal (swine) model to recapitulate human diseases, it is essential to characterize species-dependent protein sequence variants, alternative RNA splicing, and post-translational modifications (PTMs), but challenges remain due to the incomplete database and lack of validation of the predicted splicing isoforms. Herein, we integrated top-down mass spectrometry (MS) with online liquid chromatography (LC) and immunoaffinity purification to comprehensively characterize miniature swine *c*TnT proteoforms, including those arising from alternative RNA splicing and PTMs. A total of seven alternative splicing isoforms of *c*TnT were identified by LC/MS from swine left ventricular tissue, with each isoform containing unphosphorylated and mono-phosphorylated proteoforms. The phosphorylation site was localized to Ser1 for the mono-phosphorylated proteoforms of *c*TnT1, 3, 4, and 6 by online MS/MS combining collisionally activated dissociation (CAD) and electron transfer dissociation (ETD). Offline MS/MS on Fourier-transform ion cyclotron resonance (FT-ICR) mass spectrometer with CAD and electron capture dissociation (ECD) was then utilized to achieve deep sequencing of mono-phosphorylated *c*TnT1 (35.2 kDa) with a high sequence coverage of 87%. Taken together, this study demonstrated the unique advantage of top-down MS in the comprehensive characterization of protein alternative splicing isoforms together with PTMs.

Keywords: Cardiac troponin, Heart disease, Proteoform, Top-down proteomics, Collisionally activated dissociation, Electron-transfer dissociation, Electron-capture dissociation

Received: 18 January 2018/Revised: 14 February 2018/Accepted: 14 February 2018/Published Online: 9 April 2018

Introduction

Cardiac troponin (*c*Tn) complex is a critical regulator that mediates the interaction between actin thin filaments and myosin thick filaments in cardiac muscle contraction and relaxation [1–6]. There are three subunits in this complex named

Ziqing Lin and Fang Guo contributed equally to this work.

Electronic supplementary material The online version of this article (https://doi.org/10.1007/s13361-018-1925-y) contains supplementary material, which is available to authorized users.

Correspondence to: Ying Ge; *e-mail:* ge2@wisc.edu

according to their functions: cardiac troponin C (*c*TnC, encoded by *TNNC1* gene), the Ca^{2+} binding subunit; cardiac troponin I (*c*TnI, encoded by *TNNI3* gene), the actomyosin ATPase inhibiting subunit; and cardiac troponin T (*c*TnT, encoded by *TNNT2* gene), the tropomyosin-binding subunit. At low concentrations of intracellular Ca^{2+}, *c*Tn keeps tropomyosin in a position blocking the myosin interaction with actin; however, at increased levels of intracellular Ca^{2+}, the allosteric conformational change in *c*Tn-tropomyosin that occurs in response to Ca^{2+} binding exposes the myosin binding sites on the actin filaments and allows for actin-myosin interactions [2, 4]. Upon cardiac injury, *c*Tn complexes are released into the circulation following cardiac cell necrosis [7, 8]. Both *c*TnT and *c*TnI are routinely tested as biomarkers in serum by an enzyme-linked immunosorbent assay with cardiac isoform-specific antibodies [7].

Among the three subunits, *c*TnT (30–35 kDa) has the most extensive alternative RNA splicing, resulting in a highly variable protein profile in different disease phenotypes [9]. Mammalian *c*TnT RNA contains a total of 17 exons, three or more of which are known to be alternatively spliced [9]. For human *c*TnT, four exons could be excluded from the complete RNA with exon 4 and exon 5 (fetal) coding sequences expressed near the N-terminus and exon 10 and exon 13 in the central region. The exclusion of one or more exons leads to 12 potential alternatively spliced isoforms expressed (P45379) according to the UniProtKB/Swiss-Prot database. Previous studies have shown that the increased exclusion or inclusion of sequences encoded by certain exons is associated with heart disease. For instance, an increase in *c*TnT isoforms lacking the exon 4 coding sequence could cause heart failure [9] and the re-expression of embryonic *c*TnT isoforms including exon 5 in the adult myocardium may contribute to the development of heart failure and reduced contractile efficiency [9, 10]. Furthermore, phosphorylation is the major post-translational modification (PTM) discovered and studied for *c*TnT [9]. Previous studies have shown that phosphorylation of *c*TnT is regulated at multiple sites by a variety of kinases [6, 9, 11]. In addition to alternative splicing and PTMs, amino acid mutations in *c*TnT have been shown to be causative in hypertrophic, dilated, and restricted cardiomyopathies [4, 12, 13].

Recently, large animal models have been increasingly used to recapitulate human heart diseases and accelerate translational research [14–16]. Among them, domestic swine (*Sus scrofa*) is an exceedingly valuable model since swine hearts are very similar to those of humans in terms of anatomy and coronary artery distribution [17]. In contrast to the conventional breeds of swine, which can typically reach 249–306 kg (550–675 lb.) and pose challenges in husbandry and handling in the biomedical research setting, the miniature swine typically weighs 68–91 kg (150–200 lb.) at equivalent maturity [18]. Moreover, miniature swine breeds have the added advantage of slower growth curves and size similar to humans [18]. At the protein level, the myofilament proteins in swine hearts have higher sequence homology to those of humans than rodents [19]. However, because of the high genetic variability [20], the entries in the swine protein database such as *c*TnT are incomplete or have yet been validated, especially compared to the well-established human and rodent database. Thus, to fully realize the potential of swine heart model in cardiovascular research, it is essential to characterize *c*TnT sequence variants, alternative RNA splicing, as well as its PTMs.

The top-down mass spectrometry (MS)-based proteomics is arguably the most powerful method in characterizing proteoforms [21], which arise from sequence variations due to alternative splicing of the mRNA transcript and mutations/polymorphisms, as well as PTMs [1, 3, 5, 22–25]. It provides a "bird's-eye" view of all existing proteoforms by directly analyzing intact proteins after separation/purification. Ions from specific proteoforms can be subsequently isolated and subjected to multiple tandem MS (MS/MS) techniques for sequence mapping and modification localization [1]. We have previously applied top-down proteomics to study the cardiac contractile proteins in vivo from human clinical samples and various animal models [5, 26–35].

In this paper, we comprehensively characterized *c*TnT proteoforms from miniature swine left ventricle (LV) by employing a top-down LC/MS-based targeted proteomics approach coupled with immunoaffinity purification. We focused on LV because of its highly significant role in cardiac function by pumping oxygenated blood to tissues all over the body. LV dysfunction leads to congestive heart failure which is the final common pathway for various cardiac disorders [36]. Various proteoforms arising from splicing events and PTMs were profiled by online liquid chromatography (LC)/MS with and without affinity purification. Seven alternatively spliced isoforms, all of which consist of un-phosphorylated and mono-phosphorylated proteoforms, were observed following affinity purification. Online MS/MS with collisionally activated dissociation (CAD) and electron transfer dissociation (ETD) [37] enabled the identification and characterization of *c*TnT proteoforms resulting from alternative splicing and PTMs. The phosphorylation site was localized to Ser1 for the mono-phosphorylated proteoforms investigated. The affinity purification largely alleviates the sample complexity after protein extraction and therefore facilitates the subsequent comprehensive proteoform characterization by LC/MS and MS/MS. Given the possibility of *c*TnT mutations throughout the backbone as well as its molecular weight over 30 kDa, offline CAD and electron capture dissociation (ECD) were then employed to achieve complete sequence coverage of the most abundant mono-phosphorylated proteoform.

Methods

Materials

All reagents were purchased from Sigma-Aldrich Inc. (St. Louis, MO, USA) unless noted otherwise. HPLC grade water, acetonitrile (ACN), ethanol (EtOH), and 98% formic acid (FA) were purchased from Fischer Scientific (Fair Lawn, NJ, USA).

Heart tissues were from the Wisconsin Miniature Swine [18] (WMS, around 6.5 months old) which were bred and maintained at the UW Swine Research and Teaching Center (Arlington, WI). The cardiac tissue excised from the left ventricle was immediately flash frozen in liquid nitrogen and stored in at − 80 °C.

Cardiac Troponin Complex Purification

Cardiac troponin complexes were purified from 6.5-month-old miniature swine LV tissue via myofilament subproteome extraction followed by immunoaffinity purification. The extraction of myofilament proteins shown in Figure 1a was described previously [32, 33]. In brief, about 400 mg of LV tissue from 6.5 months old swine was homogenized in 4 mL wash buffer (5 mM NaH_2PO_4 and 5 mM Na_2HPO_4 at pH 7.0, 100 mM NaCl, 5 mM $MgCl_2$, 1% Triton X-100, 0.5 mM EGTA, 1 mM PMSF, 5 mM DTT) and centrifuged at 5000 rcf for 20 min at room temperature. The pellet was collected for a second wash with the same procedures. The remaining pellet after two washes was resuspended in 6 mL extraction buffer (25 mM Tris at pH 7.5, 700 mM LiCl, 0.1 mM $CaCl_2$, 5 mM EGTA, 1 mM PMSF, 5 mM DTT) and incubated for 40 min at 4 °C, followed by centrifugation at 21,000 rcf for 30 min at 4 °C, and the supernatant was collected for another centrifugation for 90 min. For the immunoaffinity purification (Figure 1b), the final supernatant was incubated in the affinity column of 0.25 mL CNBr-activated Sepharose CL-4B conjugated with 1.25 mg monoclonal *c*TnI antibody (MG4 and 14G5, HyTest Ltd., Turku, Finland) for 40 min at 4 °C. After two washes with extraction buffer (0.8 mL each), the swine *c*Tn complex was eluted in six fractions, each with 0.4 mL glycine-HCl (pH 2.0) into 40 µL 1.0 M MOPS (pH 10.0) for immediate pH neutralization. Purified *c*Tn complex was mainly present in fractions 2 and 3 according to the SDS-PAGE results as shown in Figure S1, Supplementary Information (SI).

Alternatively, myofilament proteins from the same miniature swine heart were extracted by HEPES and TFA buffers for individual *c*TnT profiling [30]. In short, 5–10 mg of swine LV tissue was homogenized in 10 volumes (µL/mg tissue) of HEPES buffer (25 mM HEPES pH 7.5, 50 mM NaF, 2.5 mM EDTA, 1 mM PMSF, 1 mM Na_3VO_4) and centrifuged at 21,100 rcf for 30 min at 4 °C. The remaining pellet was further homogenized in 10 volumes of TFA solution (1% TFA, 2 mM TCEP) and centrifuged at 21,100 rcf for 45 min at 4 °C. The final supernatant was collected for direct LC/MS analysis.

Top-Down Analysis of Cardiac Troponin T

Immunoaffinity-purified swine *c*Tn complex was desalted using a 10-kDa molecular weight cutoff filter with 0.1% FA in water. Online LC/MS analysis (Figure 1c) was carried out using a nanoAcquity ultra-high pressure LC system (Waters, Milford,

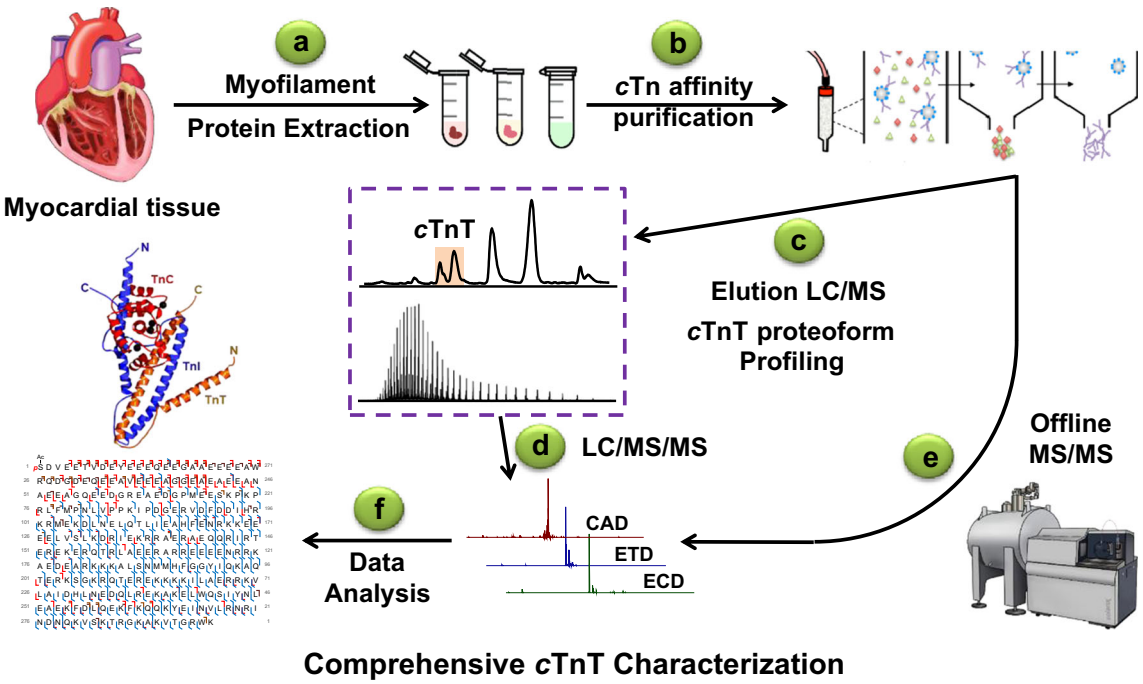

Figure 1. Characterization of swine *c*TnT proteoforms by top-down targeted proteomics. Schematic illustrating the overall workflow: (a) Myofilament subproteome extracted from swine LV tissue; (b) Tn complex purified by immunoaffinity purification; (c) *c*TnT alternative splicing and PTMs profiled by LC/MS; (d) LC/MS/MS for *c*TnT proteoform identification and PTM localization; (e) deep sequencing of specific *c*TnT proteoform by offline MS/MS with multiple dissociation methods; and (f) data analysis combining both online and offline MS/MS to achieve comprehensive characterization of swine *c*TnT proteoforms

MA, USA) coupled to high-resolution maXis II ETD and impact II quadrupole time-of-flight (Q-TOF) mass spectrometers (Bruker, Bremen, Germany). Five microliters of the desalted sample was loaded on a home-packed PLRP column (PLRP-S, 200 mm bed length, 0.5 mm i.d., 5 μm particle size, 1000 Å pore size, Agilent). Swine *c*Tn subunits were eluted by a 60-min gradient of 5 to 95% mobile phase B (mobile phase A: 0.1% FA in water, mobile phase B: 0.1% FA in 50:50 ACN/EtOH) at a flow rate of 12 μL/min. Mass spectra were taken from maXis II ETD at a scan rate of 1 Hz over 500–3000 *m/z* range. TFA extracts were diluted 20 times and analyzed on impact II with the same parameters. Online targeted LC/MS/MS of CAD and ETD (Figure 1d) was performed on maXis II ETD with the selected charge states of mono-phosphorylated proteoforms (37+ to 44+) of *c*TnT1, *c*TnT3, *c*TnT4, and *c*TnT6 at 1 Hz over 200–2000 *m/z* range from the affinity purified samples. The isolation window was set to 3 *m/z*. The collision direct current (DC) bias was fixed to 14 V for CAD (nitrogen as collision gas). The precursor ion accumulation was set to 900 ms with a reagent (3,4-hexanedione) injection duration of 10 ms and an additional 2 ms reaction for ETD.

Offline MS/MS analysis (Figure 1e) of mono-phosphorylated *c*TnT1 deep sequencing was performed with direct infusion of the affinity-purified samples after desalting, mixed with two volumes of 0.1% FA in ACN on a 12-T solariX XR (Bruker, Bremen, Germany) Fourier-transform ion cyclotron resonance (FT-ICR) mass spectrometer equipped with a nano-electrospray ionization source (Triversa NanoMate, Advion BioSciences, Ithaca, NY). The size of transients was set to 2 M with the mass range of 200–2500 *m/z* (~ 2.2 s transient length) for all MS/MS experiments acquired on the Fourier-transform mass spectrometer Fourier-transform mass spectrometer (FTMS). Each MS/MS spectrum was the sum of 200–2000 transients. The isolation window was set to 3 *m/z*. The collision DC bias for CAD ranged from 7 to 15 V (Argon as collision gas), and the ECD bias was tested 0.2–0.8 V.

Data Analysis

The LC/MS data was processed and analyzed using DataAnalysis software (Bruker Daltonics). Chromatograms shown were smoothened by Gauss algorithm with a smoothing width of 1.02 s. Mass spectra for swine *c*TnT proteoform profiling were deconvoluted using the Maximum Entropy algorithm incorporated in the DataAnalysis software. The resolving power for maximum entropy deconvolution was set to 80,000 for maXis II ETD and 50,000 for Impact II. Most abundant isotopomers of each proteoform were used to calculate the mass errors compared to the theoretical masses from *c*TnT sequences. All intact masses in this paper are reported as the most abundant masses, whereas all masses in MS/MS are reported as the monoisotopic masses for fragment assignment.

Online LC/MS/MS data was output as a .msalign file from the DataAnalysis software for *c*TnT identification using MS-Align+ [38]. The swine protein database (34,524 entries) from UniProtKB/Swiss-Prot (download date 05/09/2017) together with the predicted swine cardiac *c*TnT alternative splicing isoforms from National Center for Biotechnology Information (NCBI, seven entries) was used for database searching. All fragments from both online and offline MS/MS were validated manually using MASH Suite Pro [39]. Fragments of *b*, *y*, *c*, *c*-1, $z^{\bullet}$, and $z^{\bullet}$ + 1 ions, using a tolerance of 15 ppm for the monoisotopic masses, were assigned after the validation (Figure 1f). For CAD experiments on mono-phosphorylated *c*TnT proteoforms, phosphorylation-preserved, loss of phosphorylation (− 80 Da), and loss of phosphate (− 98 Da) fragments were observed, whereas only phosphorylation-preserved fragments were detected for ETD and ECD experiments. Multiple spectra of CAD, ETD, and ECD experiments on different charge states were combined to reach the final sequence coverage.

Results and Discussion

LC/MS Analysis of Miniature Swine cTnT Proteoforms

The online LC/MS analysis of the affinity-purified *c*Tn shows all three subunits, *c*TnT, *c*TnI, and *c*TnC, eluted with the increase of organic mobile phase (Figure 2a). Some minor chromatographic peaks were also observed, probably resulting from residual protein impurity and small molecules during the sample preparation. Together with the SDS-PAGE results (Figure S1), high purity of swine *c*Tn complex has been achieved by using anti-human *c*TnI monoclonal antibody due to the high sequence homology of *c*TnI from the two species [33]. Swine *c*TnT was separated into multiple peaks according to the total ion chromatogram in the highlighted areas of Figure 2a. By averaging the mass spectra over this retention window, seven *c*TnT alternative splicing isoforms with various abundances were observed in the deconvoluted mass spectrum of Figure 2b (individual spectra shown in Figure S2). Each *c*TnT isoform contains two major peaks, presumably un-phosphorylated and mono-phosphorylated forms based on the accurate Δmass of 79.97 Da between the two proteoforms in each set and their very similar patterns as in vivo *c*TnT proteoforms observed in human and mouse LV tissues [32]. Therefore, the observed isoforms were annotated as *c*TnT1–7 in accordance with their molecular masses from the largest to the smallest.

Despite the observation of multiple *c*TnT proteoforms, it remained difficult to identify their sequences since none of the proteoform masses among *c*TnT1–7 matched any entry in the swine UniProtKB/Swiss-Prot database, even after considering potential modifications such as N-terminal Met truncation, N-terminal acetylation, and phosphorylation. Fortunately, we were able to find the model reference sequences based on computational predictions from NCBI nucleotide database that match the observed *c*TnT proteoforms. After N-terminal Met truncation, common acetylation observed at the new N-terminal Ser1 [40], and optional mono-phosphorylation, *c*TnT1, 2, 3, 4, and 6 have the same masses as alternative RNA splicing isoforms X1 (NM_001353839.1), X2

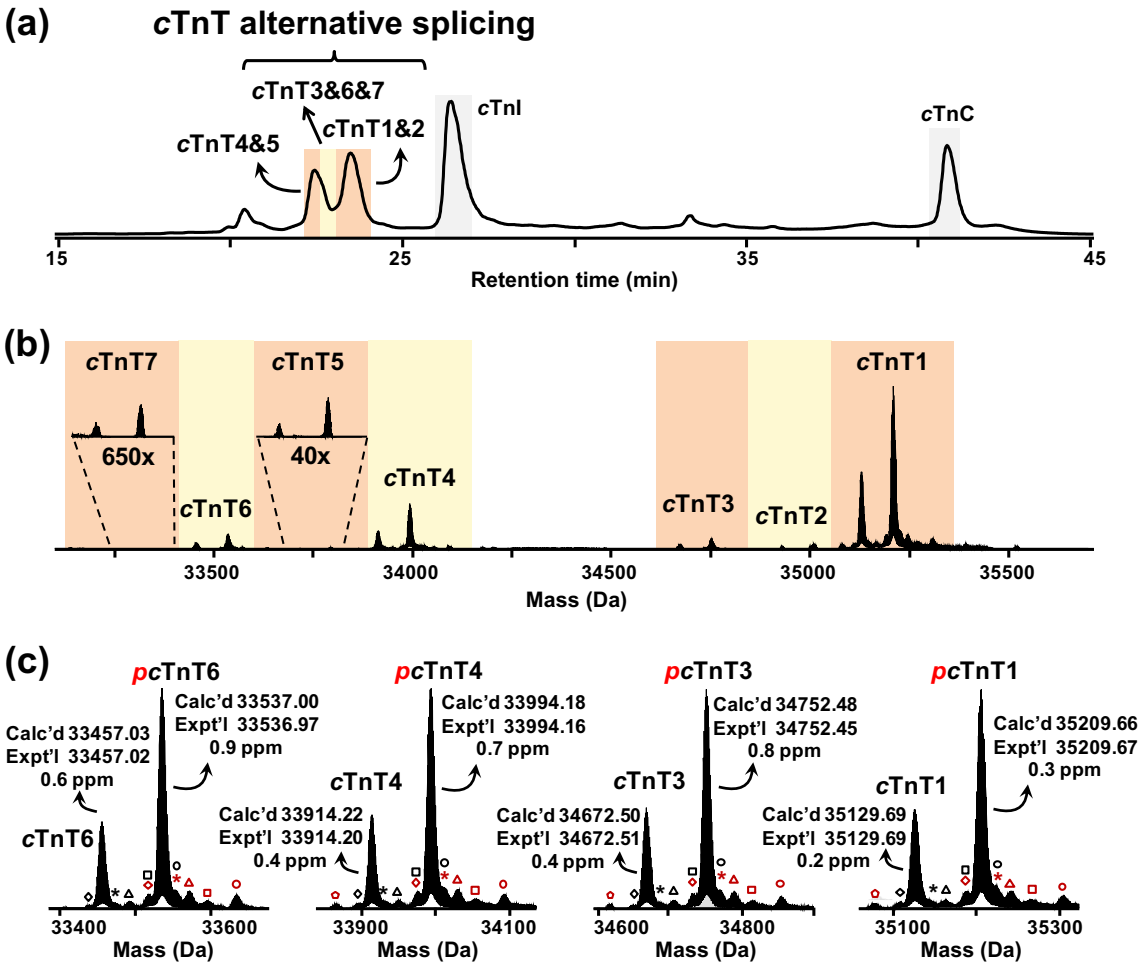

Figure 2. LC/MS analysis of *c*TnT proteoforms. (**a**) LC/MS total ion chromatogram of immunoaffinity-purified *c*Tn complex from swine LV tissue extract. (**b**) Deconvoluted mass spectrum showing seven alternative splicing isoforms of *c*TnT detected in swine LV. (**c**) Zoomed-in deconvoluted mass spectra of selected proteoforms arising from alternative splicing and PTMs. Mono-phosphorylated proteoforms were indicated as red italic p. Calc'd: theoretical most abundant mass calculated based on NCBI nucleotide database; Expt'l: experimental most abundant mass after maximum entropy deconvolution; symbols: (asterisk) + 16 Da oxidation, (triangle) + 38 Da potassium adduct, (circle) + 98 Da phosphate adduct, (square) + 62 Da adduct, (diamond) - 18 Da, (pentagon) -128 Da C-terminal Lys truncation (black: adducts from un-phosphorylated proteoforms, dark red: adducts from mono-phosphorylated proteoforms)

(NM_001353842.1), X3 (NM_001353844.1), X4 (NM_001353845.1), and X6 (NM_001257353.1), respectively, currently available in the database, while *c*TnT5 and 7 matched X5 (XM_013980114.1) and X7 (XM_013980115.1), respectively, based on the previous *Sus scrofa* build 4.3 [41]. The alignment of these alternatively spliced sequences with in vivo human and mouse *c*TnT isoforms previously reported [32] is included in Figure S3. The sequences of *c*TnT among mouse, swine, and human have high homology (79.9% overall; Figure S3), where the most abundant swine *c*TnT isoform 1 shows higher sequence homology with that of human (88.2%, swine *c*TnT1 vs. human *c*TnT6), compared to that of mouse (86.9%, mouse *c*TnT3 vs. human *c*TnT6). Figure 2c shows the top four alternative splicing isoforms with the highest MS intensities and their corresponding un-phosphorylated and mono-phosphorylated proteoform masses within 1 ppm error from the theoretical values. Some minor non-covalent adducts and neutral losses also exist as labeled in Figure 2c. The complete list of identified swine *c*TnT proteoforms is found in Table S1 by accurate mass match. This is the first time that multiple isoforms of *c*TnT were confirmed in miniature swine LV tissue. However, there might be isoform heterogeneity (in terms of species and relative abundances) in different chambers, which necessitates further investigation. It is also noteworthy that although the MS intensities of *c*TnT isoforms from alternative RNA splicing could reflect their relative abundances, the quantification by directly comparing MS intensities within the sample might not be accurate since the polarity, electrospray ionization efficiency, and MS detection from different alternatively spliced isoforms can be significantly altered by the exclusion of sequences encoded by multiple exons.

We next investigated if these isoforms can be detected without the affinity purification (HEPES and TFA extraction protocol [30]). We used *c*TnT of the same LV tissue to compare the two methods. The *c*TnT1, 3, 4, and 6 proteoform

patterns in Figure S4 by direct LC/MS analysis of the myofilament extract are highly consistent with those after the affinity purification (Figure 2b) in terms of the relative MS intensities of both alternative splicing sets and their phosphorylation levels, proving that the immunoaffinity purification successfully captured the major *c*TnT proteoforms without bias. Meanwhile, the complexity was greatly reduced after the purification compared to the whole myofilament subproteome extract (LC chromatograms; Figure 2a vs Figure S4a). As a result, the signal to noise ratios (S/N) of mutually observed *c*TnT proteoforms were higher and low abundant isoforms *c*TnT2, 5, and 7 excluding exon 13 coding sequence were only detected after the affinity purification. Direct online LC/MS of the myofilament extract is suitable for the screening purpose of abundant proteoforms with limited amounts of samples (~ 5 mg), whereas the immunoaffinity purification allows for the detection of *c*TnT proteoforms of low abundances.

Characterization of Mono-phosphorylated cTnT Proteoforms

After *c*TnT proteoform profiling, we sought to use online MS/MS of the affinity purified *c*TnT to characterize *c*TnT phosphorylation sites by both ETD and CAD. We first carried out targeted ETD experiments on the mono-phosphorylated proteoforms of swine *c*TnT1, 3, 4, and 6, since ETD preserves labile PTMs including phosphorylation [24, 37]. The fragment ions from the averaged ETD spectra of each targeted proteoform were output into one file from DataAnalysis and searched against the UniprotKB/Swiss-Prot *Sus scrofa* database together with the seven alternatively spliced *c*TnT sequences using MSAlign+ [38]. The searching results in Figure S5 unambiguously confirmed the identification of these *c*TnT proteoforms as X1, X3, X4, and X6. We subsequently examined the fragment ions in each ETD spectrum by MASH Suite Pro [39]. As shown in Figure 3, online targeted ETD yielded rich backbone cleavage of $z^{\bullet}$ ions close to the C-terminus for all four proteoforms investigated, and some degrees of cleavage in the middle range with *c* ions for mono-phosphorylated *c*TnT1, 4, and 6. All *c* ions observed were mono-phosphorylated without any detectable un-phosphorylated counterparts and all $z^{\bullet}$ ions were in their un-phosphorylated forms, which implied that the phosphorylation site could be close to the N-terminus. However, online ETD on an LC time scale alone is not sufficient to localize the phosphorylation site of swine *c*TnT. The lack of fragments close to the N-terminus is probably due to the highly acidic nature of mono-phosphorylated *c*TnT proteoforms in this region. The negatively charged phosphate together with the acidic Glu and Asp residues with low electron affinity could suppress fragmentation [42], or there might not be a positive net charge for MS to detect in positive ion mode even if fragments were produced [43].

Therefore, we performed the complementary CAD experiments on the mono-phosphorylated *c*TnT1, 3, 4, and 6. The energy transfer process via collisions in CAD cleaves the weakest peptide bonds, resulting in *b* and *y* fragment ions in proteins and peptides [1, 44]. For labile modification like phosphorylation, phosphate neutral loss (-H_3PO_4, 98 Da) exclusively occurs during CAD of small peptides [45]. In the case of intact proteins on the other hand, phosphorylation could be partially preserved in the fragmentation process [24]. Moreover, the formation of *b* ions introduces a carbonyl cation ($C{\equiv}O^{+}$) [1, 44] that could potentially mitigate the lack of positive charge sites close to N-terminus. Indeed, a series of singly charged phosphorylation-preserved and phosphate-lost (− 98 Da) *b* ions were observed among CAD fragments for mono-phosphorylated *c*TnT1, 3, 4, and 6, accompanied by minor phosphorylation loss (-HPO_3, 80 Da) shown in Figure 3. The presence of phosphorylated *b* ions very close to the N-terminus, for example, mono-phosphorylated b_3, b_4, b_5 for *c*TnT1, 3, 4, and mono-phosphorylated b_4, b_5 for *c*TnT6, indicates that the acetylated terminal Ser1 is phosphorylated, given that it is the only potential phosphorylation site among the first five amino acid residues in each alternatively spliced isoform.

Furthermore, we also observed large *y* ions by peptide bond cleavages in exon 2 and 5 encoded regions for mono-phosphorylated *c*TnT1, 4, and 6. The representative y_{290} (-*c*TnT1), y_{282} (*c*TnT4), and y_{277} (*c*TnT6) ions (Figure 3) are all un-phosphorylated absent of the corresponding mono-phosphorylated species or their potential phosphate loss (− 98 Da) forms, which confirm that there is minimum phosphorylation from Thr6 to the C-terminus. The evidences prove that Ser1 is predominantly phosphorylated for swine mono-phosphorylated *c*TnT1, 4, and 6, in agreement with the previous results that Ser1 was identified as the nearly exclusive phosphorylation site in human and mouse *c*TnT in vivo [32]. CAD of mono-phosphorylated *c*TnT3 yielded small phosphorylated *b* ions to confirm Ser1 as one major phosphorylation site but did not produce large detectable *y* ions to exclude other possible phosphorylation sites, due to the low precursor ion intensity with clean isolation as it was co-eluted with *c*TnT4. Overall, the sequence coverages of *c*TnT1, 3, 4, and 6 combining online ETD and CAD are 27, 16, 24, and 30%, respectively.

Other proteoforms *c*TnT2, 5, and 7 were too low in abundances (Figure 2; Figure S2) for MS/MS. Yet, the major phosphorylation sites of *c*TnT2, 3, 5, and 7 are most likely to be Ser1 based on the sequence homology of these alternative RNA splicing isoforms (Figure S3). The conserved phosphorylation site on Ser1 of swine *c*TnT is consistent with its well-known structure of extended N-terminal [46], which can be directly accessed by kinases. Other identified phosphorylation sites by multiple kinases from in vitro and ex vivo tests could be specific to diseased cardiomyocytes [9]. It is also possible that the occupancies of other sites in vivo for healthy hearts are extremely low (i.e., ~ 1%), which is beyond the detection limit of the current method. We have also observed that HPO_3 loss occurred for the *b* ions during CAD of *c*TnT isoforms,

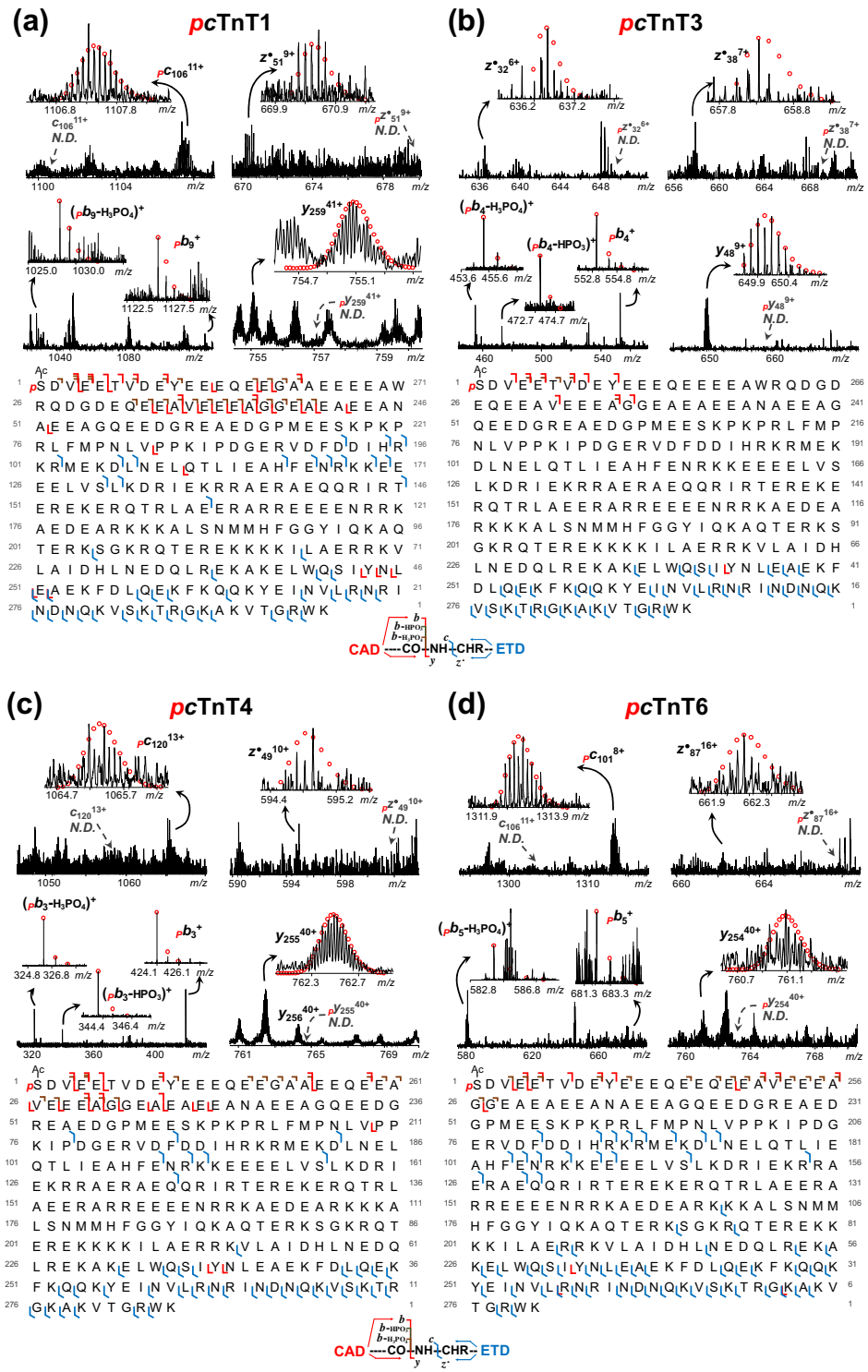

Figure 3. Online LC/MS/MS localizing the phosphorylation site to Ser1 for swine mono-phosphorylated *c*TnT proteoforms. Representative ETD and CAD fragment ions and sequence maps of (**a**) mono-phosphorylated *c*TnT1, sequence coverage 27% (79/294 bond cleavage); (**b**) mono-phosphorylated *c*TnT3, sequence coverage 16% (46/289 bond cleavage); (**c**) mono-phosphorylated *c*TnT4, sequence coverage 24% (67/284 bond cleavage); and (**d**) mono-phosphorylated *c*TnT6, sequence coverage 30% (84/279 bond cleavage). Only phosphorylation-preserved fragments were observed in ETD, whereas all phosphorylation-preserved, phosphorylation-lost (– 80 Da), and phosphate-lost (– 98 Da) fragments were detected in CAD. Italic p phosphorylation, Ac acetylation, N.D. not detected

consistent with those in human and mouse [32]. Such fragments were predominantly observed in the case of human *c*TnI (Ser22, 23) [47]. However, the fragmentation involving phosphorylation in different regions might depend on their individual sequences which require a further systematic investigation.

Deep Sequencing of Mono-phosphorylated cTnT1

Given the possibility of *c*TnT sequence variants throughout the backbone in cardiac diseases [4, 13], it would be beneficial to obtain deep *c*TnT sequence coverages to monitor any potential variances. The reason of limited *c*TnT sequence coverage around or below 30% by online LC/MS/MS is the short elution time (less than 2 min) on the LC scale which is insufficient for the low-abundance fragment ions to be accumulated. Therefore, we utilized offline direct infusion MS/MS on FTMS of swine mono-phosphorylated *c*TnT1 as it is the most abundant proteoform observed (Figure 2), aiming to achieve complete sequence coverage of this 35.2 kDa proteoform. First, we performed ECD on mono-phosphorylated *c*TnT1 at *m*/*z* 1174.7 (charge state 30+) with 0.80 V electron DC bias. The single spectrum of 2000 transients provided 32 *c* ions and 118 $z^{\bullet}$ ions and a sequence coverage of 47% of this proteoform (Figure S6a), which is already significantly higher than the coverage of all the online MS/MS spectra combined. After being normalized to their charge states, the intensities of the same fragments from multiple charge states were summed, followed by a second normalization to the most abundant fragment. From the diagram plotted in Figure 4a, extensive $z^{\bullet}$ ions (all un-phosphorylated) were observed with the most abundant fragments close to the C-terminus. The abundances of $z^{\bullet}$ ions gradually decreased as the ions get larger. A small portion of *c* ions (all phosphorylated) was also present in the middle region similar to the online ETD results. We speculated that the highly charged large fragment ions were mostly likely to undergo secondary fragmentation at the electron energy of 0.80 V. In fact, 50 more large *c* ions (10–30 kDa) were obtained by using 0.32 V electron energy shown in Figure 4b. The combination of 82 *c* ions and 100 $z^{\bullet}$ ions yields a sequence coverage of 50% at this electron energy (Figure S6b).

However, there were still no fragment ions detected close to the N-terminus as ECD and ETD share similar fragmentation mechanisms [37]. Thus, we adapted offline CAD to acquire fragments in this region. The phosphorylation-preserved and phosphate-lost ($-H_3PO_4$) *b* ions were constantly found in offline CAD (Figure S7) with multiple collision energies of the same precursor ions (charge state 29+, *m*/*z* 1215.1), accompanied by some minor phosphorylation-lost ($-HPO_3$) *b* ions. Both phosphorylation-preserved and phosphate-lost fragments are informative in locating the phosphorylation site; the neutral loss of HPO_3, nevertheless, generated fragments that could not be differentiated from those resulting from fragmentation of un-phosphorylated *c*TnT1. Only phosphorylation-preserved and phosphate-lost *b* ions are then compared in Figure 4c–e. More phosphorylation-preserved *b* ions were produced at a collision energy of 7.0 V in terms of both cleavage sites and relative abundances, whereas phosphate-lost fragments dominated *b* ions at 15 V. For *y* ions, all fragments were in un-phosphorylated form as the exclusive phosphorylation site has been pinpointed to Ser1 (Figs. 3 and 4). A variety of large *y* ions were generated at 7.0 V, whereas fragments of *y* ions in the sequence encoded by exon 6 were favored when the collision energy increased. More *y* ions closer to the C-terminus also occurred in 10 and 15 V experiments.

To achieve high sequence coverage, the fragment ions can be manipulated by screening electron energy in ECD and collision energy in CAD on multiple charge states. With 20 offline ECD and 21 offline CAD experiments carried out in addition to the online MS/MS results, we were able to achieve 87% sequence coverage of mono-phosphorylated *c*TnT1 (35.2 kDa molecular weight, 256/294 amino acid bond cleaved) shown in Figure 5. The whole sequence map contains a total of 108 *b* ions, 101 *y* ions, 106 *c* ions, and 162 $z^{\bullet}$ ions with 53 *b*/*y* and 78 *c*/$z^{\bullet}$ complementary fragment pairs. We believe with such high sequence coverage that any amino acid variants of *c*TnT could be potentially localized for abundant proteoform changes in cardiac diseases, although relatively large sample amount is needed for obtaining multiple MS/MS spectra toward the near complete sequence coverage, which may not be feasible for clinical samples where the tissue source is scarce. It also showcased the power of top-down targeted proteomics in characterizing protein modifications to within one amino acid residue.

Here, our top-down MS/MS data unambiguously identified the phosphorylation site at Ser1, which is consistent with our previous studies which also unequivocally identified Ser1, as the phosphorylation for human, and mouse *c*TnT [32]. Owing to its highly charged residues, the N-terminal region of *c*TnT adopts an extended conformation so that Ser1 residue can be easily accessible to kinase activities. Early studies on *c*TnT also determined that Ser1 was the predominant phosphorylation site in rabbit fast skeletal TnT and bovine *c*TnT [48, 49]. This demonstrates that phosphorylation of Ser1 (or Ser2 if taking in consideration of the N-terminal Met which was removed post-translationally) is highly conserved among different species. Nevertheless, the specific kinase responsible for Ser 1 phosphorylation and its physiological role remain enigmas [50].

In addition to Ser 1, previous studies have shown that phosphorylation of *c*TnT is regulated at multiple sites by a variety of kinases, such as Thr197, Ser201, Thr206, and Thr287 by protein kinase C (PKC) [51], Ser278 and Thr287 by Rho-A-dependent protein kinase (ROCK-II) [52], Thr197 and Ser201 by apoptosis signal-regulating kinase (ASK-1) [53], and Thr206 by Raf-1 [54]. Phosphorylation related to PKC is believed to be critical in the

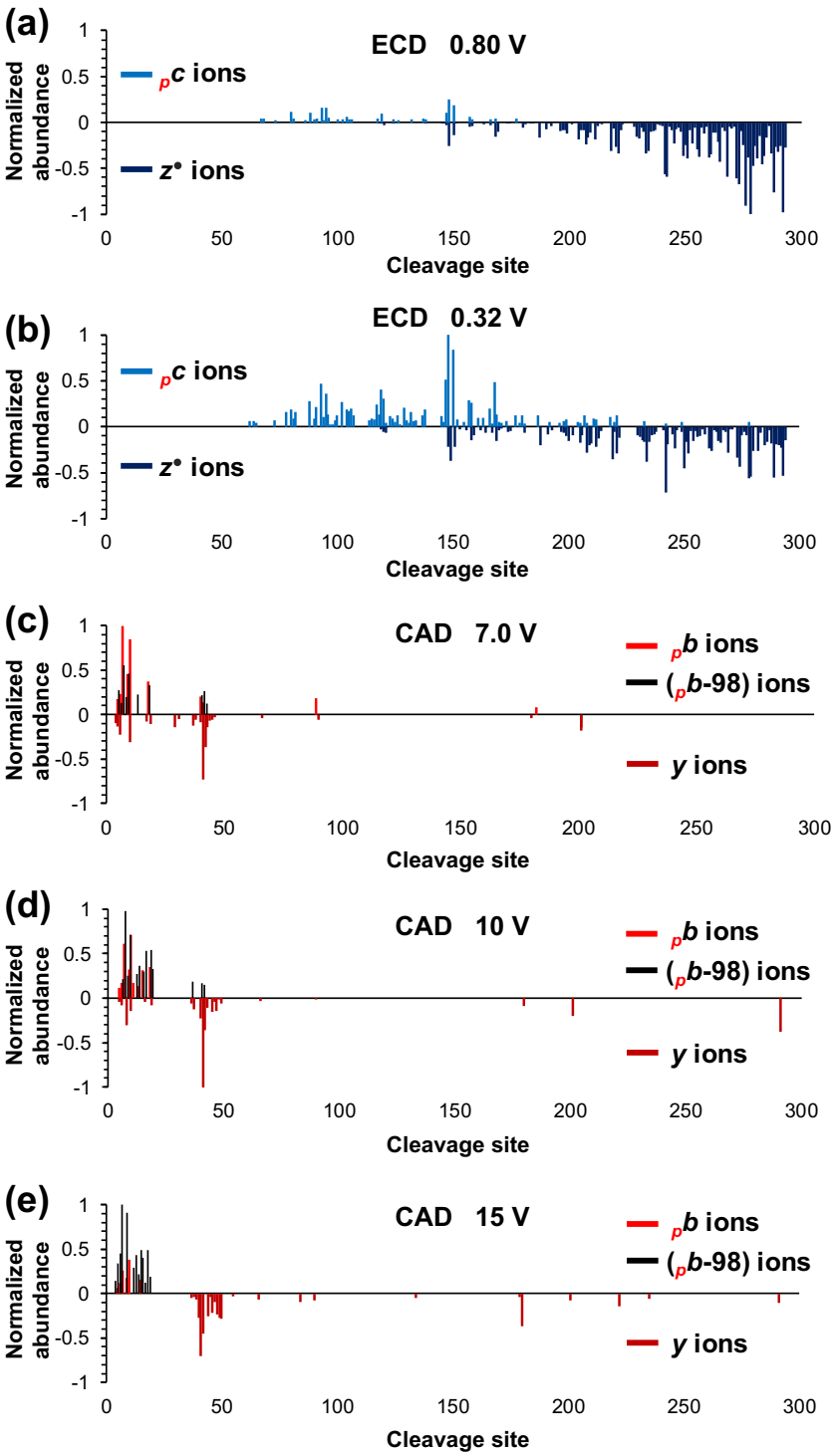

Figure 4. Offline MS/MS of swine mono-phosphorylated *c*TnT1 showing variable sequence coverage and relative abundances of fragment ions. ECD of precursor ion *m/z* 1174.7 (30+) with (**a**) 0.80 V and (**b**) 0.32 V electron DC bias, 2000 transients; CAD of precursor ion *m/z* 1215. 2 (29+) with (**c**) 7.0 V, (**d**) 10 V, and (**e**) 15 V collision DC bias, 300 transients. All assigned fragments (top 5 isotopmer) were first normalized to their charge states. The sums of ion intensities from different charge states of the same fragments were subsequently normalized to the most abundant fragment in each MS/MS experiment. *c* ions, light blue; $z^{\bullet}$ ions, dark blue; phosphorylation-preserved *b* ions, red; phosphate-lost (– 98 Da) *b* ions, black; *y* ions, dark red; phosphorylation, italic p

development of cardiac hypertrophy or heart failure based predominantly on in vitro and ex vivo results [9]. However, these phosphorylation sites in its central and C-terminal regions are not well conserved among different

Figure 5. Fragment ion map of mono-phosphorylated *c*TnT1 combining online and offline MS/MS. The overall sequence coverage was 87% (256/294 amino acid bond cleaved). A total of 108 *b* ions, 101 *y* ions, 106 *c* ions, and 162 $z^{\bullet}$ ions were observed with 53 *b*/*y* and 78 *c*/$z^{\bullet}$ complementary fragment pairs. Only phosphorylation-preserved fragments were detected in ECD and ETD, whereas all phosphorylation-preserved, loss of phosphorylation (– 80 Da), and loss of phosphate (– 98 Da) fragments were observed in CAD. Italic p phosphorylation, Ac acetylation

species and questions remain whether they are phosphorylated in vivo under physiological conditions [50].

Conclusions

In summary, we have comprehensively characterized the miniature swine LV *c*TnT proteoforms in terms of alternative splicing, phosphorylation, and deep sequencing using targeted top-down proteomics. Seven alternative RNA splicing isoforms, un-phosphorylated and mono-phosphorylated *c*TnT1–7, were observed and identified by online LC/MS integrated with immunoaffinity purification. *c*TnT1 remained the most abundant alternatively spliced isoform in miniature swine LV at 6.5 months old. *c*TnT5 and 7 of low abundances were only observed after the affinity purification with lower complexity compared to the whole myofilament extract. Phosphorylation, the main PTM of *c*TnT, was unambiguously localized to Ser1 of *c*TnT1, 4, and 6 according to online LC/MS/MS ETD and CAD results. The major phosphorylate sites of *c*TnT2, 3, 5, and 7 are most likely to be Ser1 based on sequence homology. Finally, by varying electron and collision energy in ECD and CAD, respectively, mono-phosphorylated *c*TnT1 was deep sequenced via offline MS/MS to achieve a sequence coverage of 87%. Any potential abundant *c*TnT sequence variations or modifications could be characterized with such high sequence coverage. Given the ample genetic diversity of miniature swine, *c*TnT isoform and PTM heterogeneity could arise from differences in various factors, including pedigree of breeds, age, anatomical location (e.g., different cardiac chambers), and disease status of the animals. Therefore, a systematic investigation on isoform switching and PTM changes should be conducted in the future work.

Acknowledgements

This work is dedicated to Professor Catherine E. Costello, the recipient of the 2017 Award for a Distinguished Contribution in Mass Spectrometry for her pioneering contributions to the development of tandem mass spectrometry of glycans and glycoconjugates. We would like to thank Bifan Chen for critical reading of this manuscript.

Funding Information

Financial support was kindly provided by NIH R01 HL109810 and HL096971 (to Y.G.). Y. G. would like to acknowledge NIH R01 GM117058 and S10 OD018475.

Compliance with Ethical Standards

All procedures were performed in accordance with the NIH Guide for the Care and Use of Laboratory Animals with protocols approved by the Animal Care and Use Committee of University of Wisconsin.

References

1. Cai, W.X., Tucholski, T.M., Gregorich, Z.R., Ge, Y.: Top-down proteomics: technology advancements and applications to heart diseases. Expert Rev. Proteomics. **13**, 717–730 (2016)
2. Ho, C.Y., Charron, P., Richard, P., Girolami, F., Van Spaendonck-Zwarts, K.Y., Pinto, Y.: Genetic advances in sarcomeric cardiomyopathies: state of the art. Cardiovasc. Res. **105**, 397–408 (2015)
3. Gregorich, Z.R., Ge, Y.: Top-down proteomics in health and disease: challenges and opportunities. Proteomics. **14**, 1195–1210 (2014)
4. Spudich, J.A.: Hypertrophic and dilated cardiomyopathy: four decades of basic research on muscle lead to potential therapeutic approaches to these devastating genetic diseases. Biophys. J. **106**, 1236–1249 (2014)
5. Peng, Y., Ayaz-Guner, S., Yu, D.Y., Ge, Y.: Top-down mass spectrometry of cardiac myofilament proteins in health and disease. Proteomics Clin. Appl. **8**, 554–568 (2014)
6. Perry, S.V., Troponin, T.: Genetics, properties and function. J. Muscle Res. Cell Motil. **19**, 575–602 (1998)
7. Babuin, L., Jaffe, A.S.: Troponin: the biomarker of choice for the detection of cardiac injury. Can. Med. Assoc. J. **173**, 1191–1202 (2005)
8. Jeremias, A., Gibson, C.M.: Narrative review: alternative causes for elevated cardiac troponin levels when acute coronary syndromes are excluded. Ann. Intern. Med. **142**, 786–791 (2005)
9. Wei, B., Jin, J.P., Troponin, T.: Isoforms and posttranscriptional modifications: evolution, regulation and function. Arch. Biochem. Biophys. **505**, 144–154 (2011)
10. Feng, H.Z., Jin, J.P.: Coexistence of cardiac troponin T variants reduces heart efficiency. Am. J. Phys. Heart Circ. Phys. **299**, H97–H105 (2010)
11. Solaro, R.J., Kobayashi, T.: Protein phosphorylation and signal transduction in cardiac thin filaments. J. Biol. Chem. **286**, 9935–9940 (2011)
12. Montgomery, D.E., Tardiff, J.C., Chandra, M.: Cardiac troponin T mutations: correlation between the type of mutation and the nature of myofilament dysfunction in transgenic mice. J. Physiol. Lond. **536**, 583–592 (2001)
13. Willott, R.H., Gomes, A.V., Chang, A.N., Parvatiyar, M.S., Pinto, J.R., Potter, J.D.: Mutations in troponin that cause HCM, DCM AND RCM:

what can we learn about thin filament function? J. Mol. Cell. Cardiol. **48**, 882–892 (2010)
14. Ye, L., Chang, Y.H., Xiong, Q., Zhang, P.Y., Zhang, L.Y., Somasundaram, P., Lepley, M., Swingen, C., Su, L.P., Wendel, J.S., Guo, J., Jang, A., Rosenbush, D., Greder, L., Dutton, J.R., Zhang, J.H., Kamp, T.J., Kaufman, D.S., Ge, Y., Zhang, J.Y.: Cardiac repair in a porcine model of acute myocardial infarction with human induced pluripotent stem cell-derived cardiovascular cells. Cell Stem Cell. **15**, 750–761 (2014)
15. Dixon, J.A., Spinale, F.G.: Large animal models of heart failure a critical link in the translation of basic science to clinical practice. Circ. Heart Fail. **2**, 262–271 (2009)
16. Hasenfuss, G.: Animal models of human cardiovascular disease, heart failure and hypertrophy. Cardiovasc. Res. **39**, 60–76 (1998)
17. Crick, S.J., Sheppard, M.N., Ho, S.Y., Gepstein, L., Anderson, R.H.: Anatomy of the pig heart: comparisons with normal human cardiac structure. J. Anat. **193**, 105–119 (1998)
18. Dominic, T.S., Armando, T., Jennifer, J.M., Dane, A.B., Krista, N.D., Folagbayi, K.A., Joan, W., Serge, D.R., Dhanansayan, S.: Miniature swine for preclinical modeling of complexities of human disease for translational scientific discovery and accelerated development of therapies and medical devices. Toxicol. Pathol. **44**, 299–314 (2016)
19. Hamdani, N., de Waard, M., Messer, A.E., Boontje, N.M., Kooij, V., van Dijk, S., Versteilen, A., Lamberts, R., Merkus, D., dos Remedios, C., Duncker, D.J., Borbely, A., Papp, Z., Paulus, W., Stienen, G.J.M., Marston, S.B., van der Velden, J.: Myofilament dysfunction in cardiac disease from mice to men. J. Muscle Res. Cell Motil. **29**, 189–201 (2008)
20. Lunney, J.K.: Advances in swine biomedical model genomics. Int. J. Biol. Sci. **3**, 179–184 (2007)
21. Smith, L.M., Kelleher, N.L., Consortium Top Down, P: Proteoform: a single term describing protein complexity. Nat. Methods. **10**, 186–187 (2013)
22. Ansong, C., Wu, S., Meng, D., Liu, X., Brewer, H.M., Deatherage Kaiser, B.L., Nakayasu, E.S., Cort, J.R., Pevzner, P., Smith, R.D., Heffron, F., Adkins, J.N., Pasa-Tolic, L.: Top-down proteomics reveals a unique protein S-thiolation switch in Salmonella typhimurium in response to infection-like conditions. Proc. Natl. Acad. Sci. U. S. A. **110**, 10153–10158 (2013)
23. Han, X., Jin, M., Breuker, K., McLafferty, F.W.: Extending top-down mass spectrometry to proteins with masses greater than 200 kilodaltons. Science. **314**, 109–112 (2006)
24. Siuti, N., Kelleher, N.L.: Decoding protein modifications using top-down mass spectrometry. Nat. Methods. **4**, 817–821 (2007)
25. Tran, J.C., Zamdborg, L., Ahlf, D.R., Lee, J.E., Catherman, A.D., Durbin, K.R., Tipton, J.D., Vellaichamy, A., Kellie, J.F., Li, M., Wu, C., Sweet, S.M., Early, B.P., Siuti, N., LeDuc, R.D., Compton, P.D., Thomas, P.M., Kelleher, N.L.: Mapping intact protein isoforms in discovery mode using top-down proteomics. Nature. **480**, 254–258 (2011)
26. Ayaz-Guner, S., Zhang, J., Li, L., Walker, J.W., Ge, Y.: In vivo phosphorylation site mapping in mouse cardiac troponin I by high resolution top-down electron capture dissociation mass spectrometry: Ser22/23 are the only sites basally phosphorylated. Biochemistry. **48**, 8161–8170 (2009)
27. Ge, Y., Rybakova, I.N., Xu, Q., Moss, R.L.: Top-down high-resolution mass spectrometry of cardiac myosin binding protein C revealed that truncation alters protein phosphorylation state. Proc. Natl. Acad. Sci. U. S. A. **106**, 12658–12663 (2009)
28. Guy, M.J., Chen, Y.-C., Clinton, L., Zhang, H., Zhang, J., Dong, X., Xu, Q., Ayaz-Guner, S., Ge, Y.: The impact of antibody selection on the detection of cardiac troponin I. Clin. Chim. Acta. **420**, 82–88 (2013)
29. Peng, Y., Chen, X., Zhang, H., Xu, Q., Hacker, T.A., Ge, Y.: Top-down targeted proteomics for deep sequencing of tropomyosin isoforms. J. Proteome Res. **12**, 187–198 (2013)
30. Peng, Y., Gregorich, Z.R., Valeja, S.G., Zhang, H., Cai, W.X., Chen, Y.C., Guner, H., Chen, A.J., Schwahn, D.J., Hacker, T.A., Liu, X.W., Ge, Y.: Top-down proteomics reveals concerted reductions in myofilament and Z-disc protein phosphorylation after acute myocardial infarction. Mol. Cell. Proteomics. **13**, 2752–2764 (2014)
31. Zhang, J., Guy, M.J., Norman, H.S., Chen, Y.C., Xu, Q.G., Dong, X.T., Guner, H., Wang, S.J., Kohmoto, T., Young, K.H., Moss, R.L., Ge, Y.: Top-down quantitative proteomics identified phosphorylation of cardiac troponin I as a candidate biomarker for chronic heart failure. J. Proteome Res. **10**, 4054–4065 (2011)
32. Zhang, J., Zhang, H., Ayaz-Guner, S., Chen, Y.C., Dong, X.T., Xu, Q.G., Ge, Y.: Phosphorylation, but not alternative splicing or proteolytic degradation, is conserved in human and mouse cardiac troponin T. Biochemistry. **50**, 6081–6092 (2011)
33. Zhang, J.A., Dong, X.T., Hacker, T.A., Ge, Y.: Deciphering modifications in swine cardiac troponin I by top-down high-resolution tandem mass spectrometry. J. Am. Soc. Mass Spectrom. **21**, 940–948 (2010)
34. Chen, Y.C., Ayaz-Guner, S., Peng, Y., Lane, N.M., Locher, M.R., Kohmoto, T., Larsson, L., Moss, R.L., Ge, Y.: Effective top-down LC/MS plus method for assessing actin isoforms as a potential cardiac disease marker. Anal. Chem. **87**, 8399–8406 (2015)
35. Dong, X.T., Sumandea, C.A., Chen, Y.C., Garcia-Cazarin, M.L., Zhang, J., Balke, C.W., Sumandea, M.P., Ge, Y.: Augmented phosphorylation of cardiac troponin I in hypertensive heart failure. J. Biol. Chem. **287**, 848–857 (2012)
36. Armstrong, P.: Left ventricular dysfunction: causes, natural history, and hopes for reversal. Heart. **84**, I15–I17 (2000)
37. Syka, J.E.P., Coon, J.J., Schroeder, M.J., Shabanowitz, J., Hunt, D.F.: Peptide and protein sequence analysis by electron transfer dissociation mass spectrometry. Proc. Natl. Acad. Sci. U. S. A. **101**, 9528–9533 (2004)
38. Liu, X., Sirotkin, Y., Shen, Y., Anderson, G., Tsai, Y.S., Ting, Y.S., Goodlett, D.R., Smith, R.D., Bafna, V., Pevzner, P.A.: Protein identification using top-down. Mol. Cell. Proteomics. **11**, M111.008524 (2012)
39. Cai, W.X., Guner, H., Gregorich, Z.R., Chen, A.J., Ayaz-Guner, S., Peng, Y., Valeja, S.G., Liu, X.W., Ge, Y.: MASH suite pro: a comprehensive software tool for top-down proteomics. Mol. Cell. Proteomics. **15**, 703–714 (2016)
40. Perrier, J., Durand, A., Giardina, T., Puigserver, A.: Catabolism of intracellular N-terminal acetylated proteins: involvement of acylpeptide hydrolase and acylase. Biochimie. **87**, 673–685 (2005)
41. Pruitt, K., Brown, G., Tatusova, T., et al.: The Reference Sequence (RefSeq) Database. 2002 Oct 9 [Updated 2012 Apr 6]. In: McEntyre J, Ostell J, editors. The NCBI Handbook [Internet]. Bethesda (MD): National Center for Biotechnology Information (US); 2002-. Chapter 18. Available from: https://www.ncbi.nlm.nih.gov/books/NBK21091/
42. Zubarev, R.A., Horn, D.M., Fridriksson, E.K., Kelleher, N.L., Kruger, N.A., Lewis, M.A., Carpenter, B.K., McLafferty, F.W.: Electron capture dissociation for structural characterization of multiply charged protein cations. Anal. Chem. **72**, 563–573 (2000)
43. Chen, B.F., Guo, X., Tucholski, T., Lin, Z.Q., McIlwain, S., Ge, Y.: The impact of phosphorylation on electron capture dissociation of proteins: a top-down perspective. J. Am. Soc. Mass Spectrom. 28, 1805–1814 (2017)
44. Wysocki, V.H., Resing, K.A., Zhang, Q.F., Cheng, G.L.: Mass spectrometry of peptides and proteins. Methods. **35**, 211–222 (2005)
45. Boersema, P.J., Mohammed, S., Heck, A.J.R.: Phosphopeptide fragmentation and analysis by mass spectrometry. J. Mass Spectrom. **44**, 861–878 (2009)
46. Biesiadecki, B.J., Chong, S.M., Nosek, T.M., Jin, J.P., Troponin, T.: Core structure and the regulatory NH2-terminal variable region. Biochemistry. **46**, 1368–1379 (2007)
47. Zabrouskov, V., Ge, Y., Schwartz, J., Walker, J.W.: Unraveling molecular complexity of phosphorylated human cardiac troponin I by top down electron capture dissociation/electron transfer dissociation mass spectrometry. Mol. Cell. Proteomics. **7**, 1838–1849 (2008)
48. Gusev, N.B., Dobrovolskii, A.B., Severin, S.E.: Isolation and some properties of troponin-T kinase from rabbit skeletal-muscle. Biochem. J. **189**, 219–226 (1980)
49. Moir, A.J.G., Cole, H.A., Perry, S.V.: Phosphorylation sites of troponin-T from white skeletal-muscle and effects of interaction with troponin-C on their phosphorylation by phosphorylase kinase. Biochem. J. **161**, 371–382 (1977)
50. Katrukha, I.A., Gusev, N.B.: Enigmas of cardiac troponin T phosphorylation. J. Mol. Cell. Cardiol. **65**, 156–158 (2013)
51. Sumandea, M.P., deTombe, P.P., Solaro, R.J.: PKC dependent regulation of myofilament function through cardiac troponin T phosphorylation. Circulation. **108**, 125–125 (2003)
52. Vahebi, S., Kobayashi, T., Warren, C.M., de Tombe, P.P., Solaro, R.J.: Functional effects of rho-kinase-dependent phosphorylation of specific sites on cardiac troponin. Circul. Res. **96**, 740–747 (2005)
53. He, X.G., Liu, Y.M., Sharma, V., Dirksen, R.T., Waugh, R., Sheu, S.S., Min, W.: ASK1 associates with troponin T and induces troponin T phosphorylation and contractile dysfunction in cardiomyocytes. Am. J. Pathol. **163**, 243–251 (2003)
54. Pfleiderer, P., Sumandea, M.P., Rybin, V.O., Wang, C.J., Steinberg, S.F.: Raf-1: a novel cardiac troponin T kinase. J. Muscle Res. Cell Motil. **30**, 67–72 (2009)